Observation of the doubly radiative decay $\eta' \to \gamma\gamma\pi^0$

M. Ablikim[1], M. N. Achasov[9,d], S. Ahmed[14], X. C. Ai[1], O. Albayrak[5], M. Albrecht[4], D. J. Ambrose[45], A. Amoroso[50A,50C], F. F. An[1], Q. An[47,38], J. Z. Bai[1], O. Bakina[23], R. Baldini Ferroli[20A], Y. Ban[31], D. W. Bennett[19], J. V. Bennett[5], N. Berger[22], M. Bertani[20A], D. Bettoni[21A], J. M. Bian[44], F. Bianchi[50A,50C], E. Boger[23,b], I. Boyko[23], R. A. Briere[5], H. Cai[52], X. Cai[1,38], O. Cakir[41A], A. Calcaterra[20A], G. F. Cao[1,42], S. A. Cetin[41B], J. F. Chang[1,38], G. Chelkov[23,b,c], G. Chen[1], H. S. Chen[1,42], J. C. Chen[1], M. L. Chen[1,38], S. Chen[42], S. J. Chen[29], X. Chen[1,38], X. R. Chen[26], Y. B. Chen[1,38], X. K. Chu[31], G. Cibinetto[21A], H. L. Dai[1,38], J. P. Dai[34,h], A. Dbeyssi[14], D. Dedovich[23], Z. Y. Deng[1], A. Denig[22], I. Denysenko[23], M. Destefanis[50A,50C], F. De Mori[50A,50C], Y. Ding[27], C. Dong[30], J. Dong[1,38], L. Y. Dong[1,42], M. Y. Dong[1,38,42], Z. L. Dou[29], S. X. Du[54], P. F. Duan[1], J. Z. Fan[40], J. Fang[1,38], S. S. Fang[1,42], X. Fang[47,38], Y. Fang[1], R. Farinelli[21A,21B], L. Fava[50B,50C], F. Feldbauer[22], G. Felici[20A], C. Q. Feng[47,38], E. Fioravanti[21A], M. Fritsch[22,14], C. D. Fu[1], Q. Gao[1], X. L. Gao[47,38], Y. Gao[40], Z. Gao[47,38], I. Garzia[21A], K. Goetzen[10], L. Gong[30], W. X. Gong[1,38], W. Gradl[22], M. Greco[50A,50C], M. H. Gu[1,38], Y. T. Gu[12], Y. H. Guan[1], A. Q. Guo[1], L. B. Guo[28], R. P. Guo[1], Y. Guo[1], Y. P. Guo[22], Z. Haddadi[25], A. Hafner[22], S. Han[52], X. Q. Hao[15], F. A. Harris[43], K. L. He[1,42], F. H. Heinsius[4], T. Held[4], Y. K. Heng[1,38,42], T. Holtmann[4], Z. L. Hou[1], C. Hu[28], H. M. Hu[1,42], J. F. Hu[50A,50C], T. Hu[1,38,42], Y. Hu[1], G. S. Huang[47,38], J. S. Huang[15], X. T. Huang[33], X. Z. Huang[29], Z. L. Huang[27], T. Hussain[49], W. Ikegami Andersson[51], Q. Ji[1], Q. P. Ji[15], X. B. Ji[1,42], X. L. Ji[1,38], L. W. Jiang[52], X. S. Jiang[1,38,42], X. Y. Jiang[30], J. B. Jiao[33], Z. Jiao[17], D. P. Jin[1,38,42], S. Jin[1,42], T. Johansson[51], A. Julin[44], N. Kalantar-Nayestanaki[25], X. L. Kang[1], X. S. Kang[30], M. Kavatsyuk[25], B. C. Ke[5], P. Kiese[22], R. Kliemt[10], B. Kloss[22], O. B. Kolcu[41B,f], B. Kopf[4], M. Kornicer[43], A. Kupsc[51], W. Kühn[24], J. S. Lange[24], M. Lara[19], P. Larin[14], H. Leithoff[22], C. Leng[50C], C. Li[51], Cheng Li[47,38], D. M. Li[54], F. Li[1,38], F. Y. Li[31], G. Li[1], H. B. Li[1,42], H. J. Li[1], J. C. Li[1], Jin Li[32], K. Li[33], K. Li[13], Lei Li[3], P. R. Li[42,7], Q. Y. Li[33], T. Li[33], W. D. Li[1,42], W. G. Li[1], X. L. Li[33], X. N. Li[1,38], X. Q. Li[30], Y. B. Li[2], Z. B. Li[39], H. Liang[47,38], Y. F. Liang[36], Y. T. Liang[24], G. R. Liao[11], D. X. Lin[14], B. Liu[34,h], B. J. Liu[1], C. X. Liu[1], D. Liu[47,38], F. H. Liu[35], Fang Liu[1], Feng Liu[6], H. B. Liu[12], HuanHuan Liu[1], HuiHui Liu[16], H. M. Liu[1,42], J. Liu[1], J. B. Liu[47,38], J. P. Liu[52], J. Y. Liu[1], K. Liu[40], K. Y. Liu[27], L. D. Liu[31], P. L. Liu[1,38], Q. Liu[42], S. B. Liu[47,38], X. Liu[26], Y. B. Liu[30], Y. Y. Liu[30], Z. A. Liu[1,38,42], Zhiqing Liu[22], H. Loehner[25], X. C. Lou[1,38,42], H. J. Lu[17], J. G. Lu[1,38], Y. Lu[1], Y. P. Lu[1,38], C. L. Luo[28], M. X. Luo[53], T. Luo[43], X. L. Luo[1,38], X. R. Lyu[42], F. C. Ma[27], H. L. Ma[1], L. L. Ma[33], M. M. Ma[1], Q. M. Ma[1], T. Ma[1], X. N. Ma[30], X. Y. Ma[1,38], Y. M. Ma[33], F. E. Maas[14], M. Maggiora[50A,50C], Q. A. Malik[49], Y. J. Mao[31], Z. P. Mao[1], S. Marcello[50A,50C], J. G. Messchendorp[25], G. Mezzadri[21B], J. Min[1,38], T. J. Min[1], R. E. Mitchell[19], X. H. Mo[1,38,42], Y. J. Mo[6], C. Morales Morales[14], N. Yu. Muchnoi[9,d], H. Muramatsu[44], P. Musiol[4], Y. Nefedov[23], F. Nerling[10], I. B. Nikolaev[9,d], Z. Ning[1,38], S. Nisar[8], S. L. Niu[1,38], X. Y. Niu[1], S. L. Olsen[32], Q. Ouyang[1,38,42], S. Pacetti[20B], Y. Pan[47,38], M. Papenbrock[51], P. Patteri[20A], M. Pelizaeus[4], H. P. Peng[47,38], K. Peters[10,g], J. Pettersson[51], J. L. Ping[28], R. G. Ping[1,42], R. Poling[44], V. Prasad[1], H. R. Qi[2], M. Qi[29], S. Qian[1,38], C. F. Qiao[42], L. Q. Qin[33], N. Qin[52], X. S. Qin[1], Z. H. Qin[1,38], J. F. Qiu[1], K. H. Rashid[49,i], C. F. Redmer[22], M. Ripka[22], G. Rong[1,42], Ch. Rosner[14], X. D. Ruan[12], A. Sarantsev[23,e], M. Savrié[21B], C. Schnier[4], K. Schoenning[51], W. Shan[31], M. Shao[47,38], C. P. Shen[2], P. X. Shen[30], X. Y. Shen[1,42], H. Y. Sheng[1], W. M. Song[1], X. Y. Song[1], S. Sosio[50A,50C], S. Spataro[50A,50C], G. X. Sun[1], J. F. Sun[15], S. S. Sun[1,42], X. H. Sun[1], Y. J. Sun[47,38], Y. Z. Sun[1], Z. J. Sun[1,38], Z. T. Sun[19], C. J. Tang[36], X. Tang[1], I. Tapan[41C], E. H. Thorndike[45], M. Tiemens[25], I. Uman[41D], G. S. Varner[43], B. Wang[30], B. L. Wang[42], D. Wang[31], D. Y. Wang[31], K. Wang[1,38], L. L. Wang[1], L. S. Wang[1], M. Wang[33], P. Wang[1], P. L. Wang[1], W. Wang[1,38], W. P. Wang[47,38], X. F. Wang[40], Y. Wang[37], Y. D. Wang[14], Y. F. Wang[1,38,42], Y. Q. Wang[22], Z. Wang[1,38], Z. G. Wang[1,38], Z. H. Wang[47,38], Z. Y. Wang[1], Zongyuan Wang[1], T. Weber[22], D. H. Wei[11], P. Weidenkaff[22], S. P. Wen[1], U. Wiedner[4], M. Wolke[51], L. H. Wu[1], L. J. Wu[1], Z. Wu[1,38], L. Xia[47,38], L. G. Xia[40], Y. Xia[18], D. Xiao[1], H. Xiao[48], Z. J. Xiao[28], Y. G. Xie[1,38], Y. H. Xie[6], Q. L. Xiu[1,38], G. F. Xu[1], J. J. Xu[1], L. Xu[1], Q. J. Xu[13], Q. N. Xu[42], X. P. Xu[37], L. Yan[50A,50C], W. B. Yan[47,38], W. C. Yan[47,38], Y. H. Yan[18], H. J. Yang[34,h], H. X. Yang[1], L. Yang[52], Y. X. Yang[11], M. Ye[1,38], M. H. Ye[7], J. H. Yin[1], Z. Y. You[39], B. X. Yu[1,38,42], C. X. Yu[30], J. S. Yu[26], C. Z. Yuan[1,42], Y. Yuan[1], A. Yuncu[41B,a], A. A. Zafar[49], Y. Zeng[18], Z. Zeng[47,38], B. X. Zhang[1], B. Y. Zhang[1,38], C. C. Zhang[1], D. H. Zhang[1], H. H. Zhang[39], H. Y. Zhang[1,38], J. Zhang[1], J. J. Zhang[1], J. L. Zhang[1], J. Q. Zhang[1], J. W. Zhang[1,38,42], J. Y. Zhang[1], J. Z. Zhang[1,42], K. Zhang[1], L. Zhang[1], S. Q. Zhang[30], X. Y. Zhang[33], Y. Zhang[1], Y. H. Zhang[1,38], Y. N. Zhang[42], Y. T. Zhang[47,38], Yu Zhang[42], Z. H. Zhang[6], Z. P. Zhang[47], Z. Y. Zhang[52], G. Zhao[1], J. W. Zhao[1,38], J. Y. Zhao[1], J. Z. Zhao[1,38], Lei Zhao[47,38], Ling Zhao[1], M. G. Zhao[30], Q. Zhao[1], Q. W. Zhao[1], S. J. Zhao[54], T. C. Zhao[1], Y. B. Zhao[1,38], Z. G. Zhao[47,38], A. Zhemchugov[23,b], B. Zheng[48,14], J. P. Zheng[1,38], W. J. Zheng[33], Y. H. Zheng[42], B. Zhong[28], L. Zhou[1,38], X. Zhou[52], X. K. Zhou[47,38], X. R. Zhou[47,38], X. Y. Zhou[1], K. Zhu[1], K. J. Zhu[1,38,42], S. Zhu[1], S. H. Zhu[46], X. L. Zhu[40], Y. C. Zhu[47,38], Y. S. Zhu[1,42], Z. A. Zhu[1,42], J. Zhuang[1,38], L. Zotti[50A,50C], B. S. Zou[1], J. H. Zou[1]

(BESIII Collaboration)

[1] Institute of High Energy Physics, Beijing 100049, People's Republic of China
[2] Beihang University, Beijing 100191, People's Republic of China
[3] Beijing Institute of Petrochemical Technology, Beijing 102617, People's Republic of China
[4] Bochum Ruhr-University, D-44780 Bochum, Germany
[5] Carnegie Mellon University, Pittsburgh, Pennsylvania 15213, USA
[6] Central China Normal University, Wuhan 430079, People's Republic of China
[7] China Center of Advanced Science and Technology, Beijing 100190, People's Republic of China
[8] COMSATS Institute of Information Technology, Lahore, Defence Road, Off Raiwind Road, 54000 Lahore, Pakistan
[9] G.I. Budker Institute of Nuclear Physics SB RAS (BINP), Novosibirsk 630090, Russia
[10] GSI Helmholtzcentre for Heavy Ion Research GmbH, D-64291 Darmstadt, Germany

[11] *Guangxi Normal University, Guilin 541004, People's Republic of China*
[12] *Guangxi University, Nanning 530004, People's Republic of China*
[13] *Hangzhou Normal University, Hangzhou 310036, People's Republic of China*
[14] *Helmholtz Institute Mainz, Johann-Joachim-Becher-Weg 45, D-55099 Mainz, Germany*
[15] *Henan Normal University, Xinxiang 453007, People's Republic of China*
[16] *Henan University of Science and Technology, Luoyang 471003, People's Republic of China*
[17] *Huangshan College, Huangshan 245000, People's Republic of China*
[18] *Hunan University, Changsha 410082, People's Republic of China*
[19] *Indiana University, Bloomington, Indiana 47405, USA*
[20] *(A)INFN Laboratori Nazionali di Frascati, I-00044, Frascati,*
Italy; (B)INFN and University of Perugia, I-06100, Perugia, Italy
[21] *(A)INFN Sezione di Ferrara, I-44122, Ferrara, Italy; (B)University of Ferrara, I-44122, Ferrara, Italy*
[22] *Johannes Gutenberg University of Mainz, Johann-Joachim-Becher-Weg 45, D-55099 Mainz, Germany*
[23] *Joint Institute for Nuclear Research, 141980 Dubna, Moscow region, Russia*
[24] *Justus-Liebig-Universitaet Giessen, II. Physikalisches Institut, Heinrich-Buff-Ring 16, D-35392 Giessen, Germany*
[25] *KVI-CART, University of Groningen, NL-9747 AA Groningen, The Netherlands*
[26] *Lanzhou University, Lanzhou 730000, People's Republic of China*
[27] *Liaoning University, Shenyang 110036, People's Republic of China*
[28] *Nanjing Normal University, Nanjing 210023, People's Republic of China*
[29] *Nanjing University, Nanjing 210093, People's Republic of China*
[30] *Nankai University, Tianjin 300071, People's Republic of China*
[31] *Peking University, Beijing 100871, People's Republic of China*
[32] *Seoul National University, Seoul, 151-747 Korea*
[33] *Shandong University, Jinan 250100, People's Republic of China*
[34] *Shanghai Jiao Tong University, Shanghai 200240, People's Republic of China*
[35] *Shanxi University, Taiyuan 030006, People's Republic of China*
[36] *Sichuan University, Chengdu 610064, People's Republic of China*
[37] *Soochow University, Suzhou 215006, People's Republic of China*
[38] *State Key Laboratory of Particle Detection and Electronics, Beijing 100049, Hefei 230026, People's Republic of China*
[39] *Sun Yat-Sen University, Guangzhou 510275, People's Republic of China*
[40] *Tsinghua University, Beijing 100084, People's Republic of China*
[41] *(A)Ankara University, 06100 Tandogan, Ankara, Turkey; (B)Istanbul Bilgi University, 34060 Eyup, Istanbul, Turkey;*
(C)Uludag University, 16059 Bursa, Turkey; (D)Near East University, Nicosia, North Cyprus, Mersin 10, Turkey
[42] *University of Chinese Academy of Sciences, Beijing 100049, People's Republic of China*
[43] *University of Hawaii, Honolulu, Hawaii 96822, USA*
[44] *University of Minnesota, Minneapolis, Minnesota 55455, USA*
[45] *University of Rochester, Rochester, New York 14627, USA*
[46] *University of Science and Technology Liaoning, Anshan 114051, People's Republic of China*
[47] *University of Science and Technology of China, Hefei 230026, People's Republic of China*
[48] *University of South China, Hengyang 421001, People's Republic of China*
[49] *University of the Punjab, Lahore-54590, Pakistan*
[50] *(A)University of Turin, I-10125, Turin, Italy; (B)University of Eastern*
Piedmont, I-15121, Alessandria, Italy; (C)INFN, I-10125, Turin, Italy
[51] *Uppsala University, Box 516, SE-75120 Uppsala, Sweden*
[52] *Wuhan University, Wuhan 430072, People's Republic of China*
[53] *Zhejiang University, Hangzhou 310027, People's Republic of China*
[54] *Zhengzhou University, Zhengzhou 450001, People's Republic of China*

[a] *Also at Bogazici University, 34342 Istanbul, Turkey*
[b] *Also at the Moscow Institute of Physics and Technology, Moscow 141700, Russia*
[c] *Also at the Functional Electronics Laboratory, Tomsk State University, Tomsk, 634050, Russia*
[d] *Also at the Novosibirsk State University, Novosibirsk, 630090, Russia*
[e] *Also at the NRC "Kurchatov Institute", PNPI, 188300, Gatchina, Russia*
[f] *Also at Istanbul Arel University, 34295 Istanbul, Turkey*
[g] *Also at Goethe University Frankfurt, 60323 Frankfurt am Main, Germany*
[h] *Also at Key Laboratory for Particle Physics, Astrophysics and Cosmology, Ministry of Education; Shanghai Key Laboratory*
for Particle Physics and Cosmology; Institute of Nuclear and Particle Physics, Shanghai 200240, People's Republic of China
[i] *Government College Women University, Sialkot - 51310. Punjab, Pakistan.*

Based on a sample of 1.31 billion J/ψ events collected with the BESIII detector, we report the study of the doubly radiative decay $\eta' \to \gamma\gamma\pi^0$ for the first time, where the η' meson is produced via the $J/\psi \to \gamma\eta'$ decay. The branching fraction of $\eta' \to \gamma\gamma\pi^0$ inclusive decay is measured to be $\mathcal{B}(\eta' \to \gamma\gamma\pi^0)_{\text{Incl.}} = (3.20 \pm 0.07(\text{stat}) \pm 0.23(\text{sys})) \times 10^{-3}$, while the branching fractions of the dominant process $\eta' \to \gamma\omega$ and the nonresonant component are determined to be $\mathcal{B}(\eta' \to \gamma\omega) \times \mathcal{B}(\omega \to \gamma\pi^0) =$

$(23.7 \pm 1.4(\text{stat}) \pm 1.8(\text{sys})) \times 10^{-4}$ and $\mathcal{B}(\eta' \to \gamma\gamma\pi^0)_{\text{NR}} = (6.16 \pm 0.64(\text{stat}) \pm 0.67(\text{sys})) \times 10^{-4}$, respectively. In addition, the $M_{\gamma\gamma}^2$-dependent partial widths of the inclusive decay are also presented.

PACS numbers: 13.40.Gp, 13.40.Hq, 13.20.Jf, 14.40.Be

I. INTRODUCTION

The η' meson provides a unique stage for understanding the distinct symmetry-breaking mechanisms present in low-energy quantum chromodynamics (QCD) [1–5] and its decays play an important role in exploring the effective theory of QCD at low energy [6]. Recently, the doubly radiative decay $\eta' \to \gamma\gamma\pi^0$ was studied in the frameworks of the linear σ model (LσM) and the vector meson dominance (VMD) model [7, 8]. It has been demonstrated that the contributions from the VMD are dominant. Experimentally, only an upper limit of the nonresonant branching fraction of $\mathcal{B}(\eta' \to \gamma\gamma\pi^0)_{\text{NR}} < 8 \times 10^{-4}$ at the 90% confidence level has been determined by the GAMS-2000 experiment [9].

In this article, we report the first measurement of the branching fraction of the inclusive $\eta' \to \gamma\gamma\pi^0$ decay and the determination of the $M_{\gamma\gamma}^2$ dependent partial widths, where $M_{\gamma\gamma}$ is the invariant mass of the two radiative photons. The inclusive decay is defined as the η' decay into the final state $\gamma\gamma\pi^0$ including all possible intermediate contributions from the ρ and ω mesons below the η' mass threshold and the nonresonant contribution from the excited vector meson above the η' mass threshold. Since the contribution from mesons above the η' threshold actually derives from the low-mass tail and looks like a contact term, we call this contribution 'nonresonant'. The branching fraction for the nonresonant $\eta' \to \gamma\gamma\pi^0$ decay is obtained from a fit to the $\gamma\pi^0$ invariant mass distribution by excluding the coherent contributions from the ρ and ω intermediate states. The measurement of the $M_{\gamma\gamma}^2$ dependent partial widths will provide direct inputs to the theoretical calculations on the transition form factors of $\eta' \to \gamma\gamma\pi^0$ and improve the theoretical understanding of the η' decay mechanisms.

II. EXPERIMENTAL DETAILS

The source of η' mesons is the radiative $J/\psi \to \gamma\eta'$ decay in a sample of 1.31×10^9 J/ψ events [10, 11] collected by the BESIII detector. Details on the features and capabilities of the BESIII detector can be found in Ref. [12].

The response of the BESIII detector is modeled with a Monte Carlo (MC) simulation based on GEANT4 [13]. The program EVTGEN [14] is used to generate a $J/\psi \to \gamma\eta'$ MC sample with an angular distribution of $1+\cos^2\theta_\gamma$, where θ_γ is the angle of the radiative photon relative to the positron beam direction in the J/ψ rest frame. The decays $\eta' \to \gamma\omega(\rho)$, $\omega(\rho) \to \gamma\pi^0$ are generated using the helicity amplitude formalism. For the nonresonant $\eta' \to \gamma\gamma\pi^0$ decay, the VMD model [7, 8] is used to generate the MC sample with $\rho(1450)$ or $\omega(1650)$ exchange. Inclusive J/ψ decays are generated with KKMC [15] generator; the known J/ψ decay modes are generated by EVTGEN [14] with branching fractions setting at Particle Data Group (PDG) world average values [16]; the remaining unknown decays are generated with LUNDCHARM [17].

III. EVENT SELECTION AND BACKGROUND ESTIMATION

Electromagnetic showers are reconstructed from clusters of energy deposits in the electromagnetic calorimeter (EMC). The energy deposited in nearby time-of-light (TOF) counters is included to improve the reconstruction efficiency and energy resolution. The photon candidate showers must have a minimum energy of 25 MeV in the barrel region ($|\cos\theta| < 0.80$) or 50 MeV in the end cap region ($0.86 < |\cos\theta| < 0.92$). Showers in the region between the barrel and the end caps are poorly measured and excluded from the analysis. In this analysis, only the events without charged particles are subjected to further analysis. The average event vertex of each run is assumed as the origin for the selected candidates. To select $J/\psi \to \gamma\eta'$, $\eta' \to \gamma\gamma\pi^0$ ($\pi^0 \to \gamma\gamma$) signal events, only the events with exactly five photon candidates are selected.

To improve resolution and reduce background, a five-constraint kinematic (5C) fit imposing energy-momentum conservation and a π^0 mass constraint is performed to the $\gamma\gamma\gamma\pi^0$ hypothesis, where the π^0 candidate is reconstructed with a pair of photons. For events with more than one π^0 candidate, the combination with the smallest $\chi^2_{5\text{C}}$ is selected. Only events with $\chi^2_{5\text{C}} < 30$ are retained. The χ^2_{5C} distribution is shown in Fig. 1 with events in the η' signal region of $|M_{\gamma\gamma\pi^0} - M_{\eta'}| < 25$ MeV ($M_{\eta'}$ is the η' nominal mass from PDG [16]). In order to suppress the multi-π^0 backgrounds and remove the mis-combined π^0 candidates, an event is vetoed if any two of five selected photons (except for the combination for the π^0 candidate) satisfies $|M_{\gamma\gamma} - M_{\pi^0}| < 18$ MeV/c^2, where M_{π^0} is the π^0 nominal mass. After the application of the above requirements, the most energetic photon is taken as the primary photon from the J/ψ decay, and the remaining two photons and the π^0 are used to reconstruct the η' candidates. Figure 2 shows the $\gamma\gamma\pi^0$ invariant mass spectrum.

Detailed MC studies indicate that no peaking background remains after all the selection criteria. The
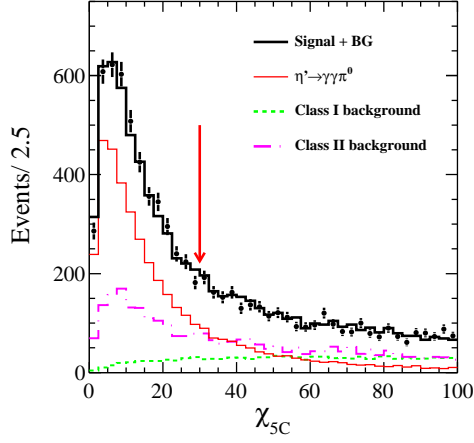
FIG. 1: Distribution of the χ^2_{5C} of the 5C kinematic fit for the inclusive η' decay. Dots with error bars are data; the heavy (black) solid-curve is the sum of signal and expected backgrounds from MC simulations; the light (red) solid-curves is signal components which are normalized to the fitted yields; the (green) dotted-curve is the class I background; and the (pink) dot-dashed-curve is the class II background.
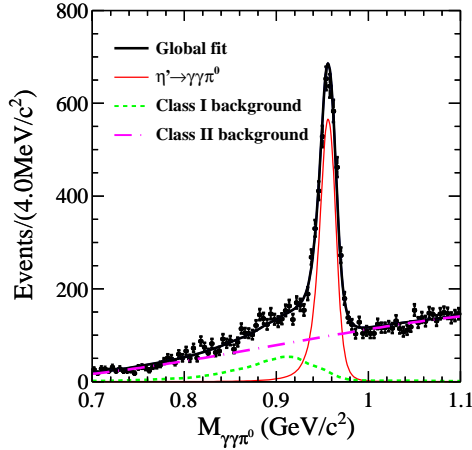

FIG. 2: Results of the fit to $M_{\gamma\gamma\pi^0}$ for the selected inclusive $\eta' \to \gamma\gamma\pi^0$ signal events. The (black) dots with error bars are the data.

sources of backgrounds are divided into two classes. Background events of class I are from $J/\psi \to \gamma\eta'$ with η' decaying into final states other than the signal final states. These background events accumulate near the lower side of the η' signal region and are mainly from $\eta' \to \pi^0\pi^0\eta$ ($\eta \to \gamma\gamma$), $\eta' \to 3\pi^0$ and $\eta' \to \gamma\gamma$, as shown as the (green) dotted curve in Fig. 2. Background events in class II are mainly from J/ψ decays to final states without η', such as $J/\psi \to \gamma\pi^0\pi^0$ and $J/\psi \to \omega\eta$ ($\omega \to \gamma\pi^0$, $\eta \to \gamma\gamma$) decays, which contribute a smooth distribution under the η' signal region as displayed as the (pink) dot-dashed curve in Fig. 2.

IV. SIGNAL YIELDS AND BRANCHING FRACTIONS

A fit to the $\gamma\gamma\pi^0$ invariant mass distribution is performed to determine the inclusive $\eta' \to \gamma\gamma\pi^0$ signal yield. The probability density function (PDF) for the signal component is represented by the signal MC shape, which is obtained from the signal MC sample generated with an incoherent mixture of ρ, ω and the nonresonant components according to the fractions obtained in this analysis. Both the shape and the yield for the class I background are fixed to the MC simulations and their expected intensities. The shape for the class II background is described by a third-order Chebychev polynomial, and the corresponding yield and PDF parameters are left free in the fit to data. The fit range is $0.70-1.10$ GeV/c^2. Figure 2 shows the results of the fit. The fit quality assessed with the binned distribution is $\chi^2/\text{n.d.f} = 108/95 = 1.14$. The signal yield and the MC-determined signal efficiency for the inclusive η' decay are summarized in Table I.

In this analysis, the partial widths can be obtained by studying the efficiency-corrected signal yields for each given $M^2_{\gamma\gamma}$ bin i for the inclusive $\eta' \to \gamma\gamma\pi^0$ decay. The resolution in $M^2_{\gamma\gamma}$ is found to be about 5×10^2 (MeV/c^2)^2 from the MC simulation, which is much smaller than 1.0×10^4 (MeV/c^2)^2, a statistically reasonable bin width, and hence no unfolding is necessary. The η' signal yield in each $M^2_{\gamma\gamma}$ bin is obtained by performing bin-by-bin fits to the $\gamma\gamma\pi^0$ invariant mass distributions using the fit procedure described above. Thus the background-subtracted, efficiency-corrected signal yield can be used to obtain the partial width for each given $M^2_{\gamma\gamma}$ interval, where the PDG value is used for the total width of the η' meson [16]. The results for $d\Gamma(\eta' \to \gamma\gamma\pi^0)/dM^2_{\gamma\gamma}$ in each $M^2_{\gamma\gamma}$ interval are listed in Table II and depicted in Fig. 3, where the contributions from each component obtained from the MC simulations are normalized with the yields by fitting to $M_{\gamma\pi^0}$ as displayed in Fig. 4.

Assuming that the inclusive decay $\eta' \to \gamma\gamma\pi^0$ can be attributed to the vector mesons ρ and ω and the nonresonant contribution, we apply a fit to the $\gamma\pi^0$ invariant mass to determine the branching fraction for the nonresonant $\eta' \to \gamma\gamma\pi^0$ decay using the η' signal events with $|M_{\gamma\gamma\pi^0} - m_{\eta'}| < 25$ MeV/c^2. In the fit, the ρ-ω interference is considered, but possible interference between the ω (ρ) and the nonresonant process is neglected. To validate our fit, we also determine the product branching fraction for the decay chain $\eta' \to \gamma\omega$, $\omega \to \gamma\pi^0$. Figure 4 shows the $M_{\gamma\pi^0}$ distribution. Since the doubly radiative photons are indistinguishable, two entries are filled into the histogram for each event. For the PDF of the coherent ω and ρ produced in $\eta' \to \gamma\gamma\pi^0$, we use $[\varepsilon(M_{\gamma\pi^0}) \times E^3_{\gamma\eta'} \times E^3_{\gamma\omega(\rho)} \times |\text{BW}_\omega(M_{\gamma\pi^0}) + \alpha e^{i\theta}\text{BW}_\rho(M_{\gamma\pi^0})|^2 \times \text{B}^2_{\eta'} \times \text{B}^2_{\omega(\rho)}] \otimes \text{G}(0, \sigma)$, where $\varepsilon(M_{\gamma\pi^0})$ is the detection efficiency determined by the MC simulations; $E_{\gamma\eta'(\omega/\rho)}$ is the energy of the transition photon in

TABLE I: Observed η' signal yields ($N^{\eta'}$) and detection efficiencies (ϵ) for inclusive $\eta' \to \gamma\gamma\pi^0$, $\eta' \to \gamma\omega(\omega \to \gamma\pi^0)$, and the nonresonant $\eta' \to \gamma\gamma\pi^0$ decays. The measured branching fractions^c in this work, comparison of values from the PDG [16] and theoretical predictions are listed. The first errors are statistical and the second ones are systematic.

	$\eta' \to \gamma\gamma\pi^0$ (Inclusive)	$\eta' \to \gamma\omega, \omega \to \gamma\pi^0$	$\eta' \to \gamma\gamma\pi^0$ (Nonresonant)
$N^{\eta'}$	$3435 \pm 76 \pm 244$	$2340 \pm 141 \pm 180$	$655 \pm 68 \pm 71$
ϵ	16.1%	14.8%	15.9%
$\mathcal{B}$ (10^{-4})	$32.0 \pm 0.7 \pm 2.3$	$23.7 \pm 1.4 \pm 1.8^a$	$6.16 \pm 0.64 \pm 0.67$
$\mathcal{B}_{\text{PDG}}$ (10^{-4})	–	21.7 ± 1.3^b	< 8
Predictions (10^{-4})	57 [7],65 [8]	–	–

^{a} The product branching fraction $\mathcal{B}(\eta' \to \gamma\omega) \cdot \mathcal{B}(\omega \to \gamma\pi^0)$. ^{b} The product branching fraction $\mathcal{B}(\eta' \to \gamma\omega) \cdot \mathcal{B}(\omega \to \gamma\pi^0)$ from PDG [16].
^{c} The product branching fraction $\mathcal{B}(\eta' \to \gamma\rho) \cdot \mathcal{B}(\rho^0 \to \gamma\pi^0)$ is determined to be $(1.92 \pm 0.16(\text{stat})) \times 10^{-4}$ using the fitted yield in Fig. 4, which is in agreement with the PDG value of $(1.75 \pm 0.23) \times 10^{-4}$ [16].

TABLE II: Results for $d\Gamma(\eta' \to \gamma\gamma\pi^0)/dM_{\gamma\gamma}^2$ (in units of keV/(GeV/c^2)^2) for thirteen intervals of $M_{\gamma\gamma}^2$. The first uncertainties are statistical and the second systematic.

$M_{\gamma\gamma}^2$ ((GeV/c^2)^2)	[0.0, 0.01]	[0.01, 0.04]	[0.04, 0.06]	[0.06, 0.09]	[0.09, 0.12]
$d\Gamma(\eta' \to \gamma\gamma\pi^0)/M_{\gamma\gamma}^2$	$3.17 \pm 0.44 \pm 0.24$	$2.57 \pm 0.18 \pm 0.19$	$2.60 \pm 0.15 \pm 0.18$	$1.87 \pm 0.12 \pm 0.14$	$1.76 \pm 0.11 \pm 0.13$
$M_{\gamma\gamma}^2$ ((GeV/c^2)^2)	[0.12, 0.16]	[0.16, 0.20]	[0.20, 0.25]	[0.25, 0.28]	[0.28, 0.31]
$d\Gamma(\eta' \to \gamma\gamma\pi^0)/M_{\gamma\gamma}^2$	$1.63 \pm 0.10 \pm 0.12$	$1.76 \pm 0.09 \pm 0.13$	$1.97 \pm 0.10 \pm 0.14$	$2.00 \pm 0.17 \pm 0.15$	$1.07 \pm 0.20 \pm 0.08$
$M_{\gamma\gamma}^2$ ((GeV/c^2)^2)	[0.31, 0.36]	[0.36, 0.42]	[0.42, 0.64]		
$d\Gamma(\eta' \to \gamma\gamma\pi^0)/M_{\gamma\gamma}^2$	$0.34 \pm 0.06 \pm 0.03$	$0.12 \pm 0.03 \pm 0.01$	$0.06 \pm 0.01 \pm 0.01$		

the rest frame of η' (ω/ρ); BW$_\omega(M_{\pi^0})$ is a relativistic Breit-Wigner (BW) function, and BW$_\rho(M_{\gamma\pi^0})$ is a relativistic BW function with mass-dependent width [18]. The masses and widths of the ρ and ω meson are fixed to their PDG values [16]. B$_{\eta'(\omega/\rho)}^2$ is the Blatt-Weisskopf centrifugal barrier factor for the $\eta'(\omega/\rho)$ decay vertex with radius $R = 0.75$ fm [19, 20], and B$_{\eta'(\omega/\rho)}^2$ is used to damp the divergent tail due to the factor $E_{\gamma\eta'(\omega/\rho)}^3$. The Gaussian function G$(0, \sigma)$ is used to parameterize the detector resolution. The combinatorial background is produced by the combination of the π^0 and the photon from the η' meson, and its PDF is described with a fixed shape from the MC simulation. The ratio of yields between the combinatorial backgrounds and the coherent sum of ρ-ω signals is fixed from the MC simulations. The shape of the nonresonant signal $\eta' \to \gamma\gamma\pi^0$ is determined from the MC simulation, and its yield is determined in the fit. The background from the class I as discussed above is fixed to the shape and yield of the MC simulation. Finally, the shape from the class II background is obtained from the η' mass sidebands (738$-$788 and 1008$-$1058 MeV/c^2), and its normalization is fixed in the fit. The $M_{\gamma\pi^0}$ mass range used in the fit is 0.20$-$0.92 GeV/c^2. In the fit, the interference phase θ between the ρ- and ω-components is allowed. Due to the low statistics of the ρ meson contribution, we fix the ratio α of ρ and ω intensities to the value for the ratio of $\mathcal{B}(\eta' \to \gamma\rho) \cdot \mathcal{B}(\rho \to \gamma\pi^0)$ and $\mathcal{B}(\eta' \to \gamma\omega) \cdot \mathcal{B}(\omega \to \gamma\pi^0)$ from the PDG [16]. Figure 4

shows the results. The yields for the vector mesons ρ, ω and their interference are determined to be (183 ± 15), (2340 ± 141), and (174 ± 92), respectively. The signal yields and efficiencies as well as the corresponding branching fractions for the $\eta' \to \gamma\omega(\omega \to \gamma\pi^0)$ and nonresonant decays are summarized in Table I.

V. SYSTEMATIC UNCERTAINTIES

The systematic uncertainties on the branching fraction measurements are summarized in Table III. The uncertainty due to the photon reconstruction is determined to be 1% per photon as described in Ref. [21]. The uncertainties associated with the other selection criteria, kinematic fit with $\chi_{5C}^2 < 30$, the number of photons equal to 5 and π^0 veto ($|M_{\gamma\gamma} - M_{\pi^0}| > 18$ MeV/c^2) are studied with the control sample $J/\psi \to \gamma\eta'$, $\eta' \to \gamma\omega$, $\omega \to \gamma\pi^0$ decay, respectively. The systematic error in each of the applied selection criteria is numerically estimated from the ratio of the number of events with and without the corresponding requirement. The corresponding resulting efficiency differences between data and MC (2.7%, 0.5%, and 1.9% , respectively) are taken to be representative of the corresponding systematic uncertainties.

In the fit for the inclusive η' decay, the signal shape is fixed to the MC simulation. The uncertainty due to
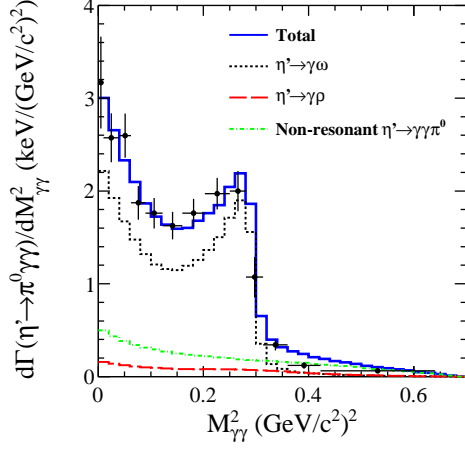
FIG. 3: Partial width (in keV) versus $M_{\gamma\gamma}^2$ for the inclusive $\eta' \to \gamma\gamma\pi^0$ decay. The error includes the statistic and systematic uncertainties. The (blue) histogram is the sum of an incoherent mixture of ρ-ω and the nonresonant components from MC simulations; the (back) dotted-curves is ω-contribution; the (red) dot-dashed-curve is the ρ-contribution; and the (green) dashed-curve is the nonresonant contribution. All the components are normalized using the yields obtained in Fig. 4.
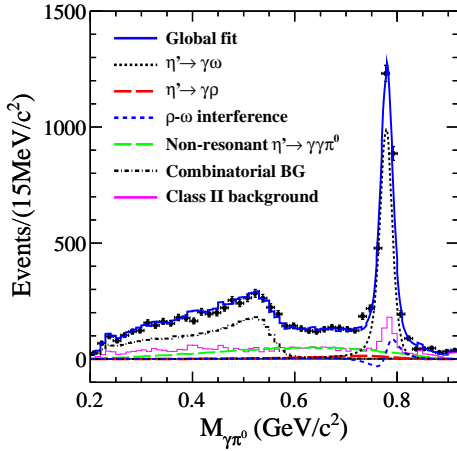
FIG. 4: Distribution of the invariant mass $M_{\gamma\pi^0}$ and fit results in the η' mass region. The points with error bars are data; the (black) dotted-curve is from the ω-contribution; the (red) long dashed-curve is from the ρ-contribution; the (blue) short dashed-curve is the contribution of ρ-ω interference; the (green) long dashed curve is the nonresonance; the (pink) histogram is from the class II background; the (black) short dot-dashed curve is the combinatorial backgrounds of $\eta' \to \gamma\omega, \gamma\rho$. The (blue) solid line shows the total fit function.

the signal shape is considered by convolving a Gaussian function to account for the difference in the mass resolution between data and MC simulation. In the fit to the $\gamma\pi^0$ distribution, alternative fits with the mass resolution left free in the fit and the radius R in the barrier factor changed from 0.75 fm to 0.35 fm are performed, and the

changes of the signal yields are taken as the uncertainty due to the signal shape.

In the fit to the $M_{\gamma\gamma\pi^0}$ distribution, the signal shape is described with an incoherent sum of contributions from processes involving ρ and ω and nonresonant processes obtained from MC simulation, where the nonresonant process is modeled with the VMD model. A fit with an alternative signal model for the different components, *i.e.* a coherent sum for the ρ-, ω-components and a uniform angular distribution in phase space (PHSP) for the non-resonant process, is performed. The resultant changes in the branching fractions are taken as the uncertainty related to the signal model. An alternate fit to the $M_{\gamma\pi^0}$ distribution is performed, where the PDF of the nonresonant decay is extracted from the PHSP MC sample. The changes in the measured branching fractions are considered to be the uncertainty arising from the signal model.

In the fit to the $M_{\gamma\pi^0}$ distribution, the uncertainty due to the fixed relative ρ intensity is evaluated by changing its expectation by one standard deviation. An alternative fit in which the ratio of yields between combinatorial backgrounds and the coherent sum of $\rho-\omega$ signals is changed by one standard deviation from the MC simulation is performed, and the change observed in the signal yield is assigned as the uncertainty. A series of fits using different fit ranges is performed and the maximum change of the branching fraction is taken as a systematic uncertainty.

The uncertainty due to the class I background is estimated by varying the numbers of expected background events by one standard deviation according to the errors on the branching fraction values in PDG [16]. The uncertainty due to the class II background is evaluated by changing the order of the Chebychev polynomial from 3 to 4 for the fit to the η' inclusive decay, and varying the ranges of η' sidebands for the fit to the $\gamma\pi^0$ invariant mass distribution, respectively.

The number of J/ψ events is $N_{J/\psi} = (1310.6 \pm 10.5) \times 10^6$ [10, 11], corresponding to an uncertainty of 0.8%. The branching fractions for the $J/\psi \to \gamma\eta'$ and $\pi^0 \to \gamma\gamma$ decays are taken from the PDG [16], and the corresponding uncertainties are taken as a systematic uncertainty. The total systematic errors are 7.1%, 7.7%, 10.8% for the inclusive decay, ω contribution and nonresonant decay, respectively, as summarized in Table III.

VI. SUMMARY

In summary, with a sample of 1.31×10^9 J/ψ events collected with the BESIII detector, the doubly radiative decay $\eta' \to \gamma\gamma\pi^0$ has been studied. The branching fraction of the inclusive decay is measured for the first time to be $\mathcal{B}(\eta' \to \gamma\gamma\pi^0)_{\text{Incl.}} = (3.20 \pm 0.07(\text{stat}) \pm 0.23(\text{sys})) \times 10^{-3}$. The $M_{\gamma\gamma}^2$ dependent partial decay widths are also determined. In addition, the branching fraction for the

TABLE III: Summary of relative systematic uncertainties (%) for the branching fraction measurements. Here $\eta'_{\rm Incl.}$, η'_ω and $\eta'_{\rm NR}$ represent the inclusive $\eta' \to \gamma\gamma\pi^0$, $\eta' \to \gamma\omega(\omega \to \gamma\pi^0)$ and nonresonant decays, respectively.

	$\eta'_{\rm Incl.}$	η'_ω	$\eta'_{\rm NR}$
Photon detection	5.0	5.0	5.0
5C kinematic fit	2.7	2.7	2.7
Number of photons	0.5	0.5	0.5
π^0 veto	1.9	1.9	1.9
Signal shape	0.5	1.5	2.3
Signal model	1.7	1.0	4.3
ρ relative intensity	–	1.3	4.9
Combinatorial backgrounds	–	1.3	0.8
Fit range	0.8	1.6	2.1
Class I background	0.1	0.2	0.6
Class II background	0.3	1.8	4.2
Cited branching fractions	3.1	3.1	3.1
Number of J/ψ events	0.8	0.8	0.8
Total systematic error	7.1	7.7	10.8

nonresonant decay is determined to be $\mathcal{B}(\eta' \to \gamma\gamma\pi^0)_{\rm NR}$ = $(6.16 \pm 0.64(\text{stat}) \pm 0.67(\text{sys})) \times 10^{-4}$, which agrees with the upper limit measured by the GAMS-2000 experiment [9]. As a validation of the fit, the product branching fraction with the omega intermediate state involved is obtained to be $\mathcal{B}(\eta' \to \gamma\omega) \cdot \mathcal{B}(\omega \to \gamma\pi^0)$ = $(2.37 \pm 0.14(\text{stat}) \pm 0.18(\text{sys})) \times 10^{-3}$, which is consistent with the PDG value [16]. These results are useful to test QCD calculations on the transition form factor, and provide valuable inputs to the theoretical understanding of the light meson decay mechanisms.

Acknowledgments

[1] J. Steinberger, Phys. Rev. **76**, 1180 (1949); S. L. Adler, Phys. Rev. **177**, 2426 (1969); J. S. Bell and R. Jackiw, Nuovo Cim. **A 60**, 47 (1969); W. A. Bardeen, Phys. Rev. **184**, 1848 (1969).
[2] J. Wess and B. Zumino, Phys. Lett. **B 37**, 95 (1971).
[3] E. Witten, Nucl. Phys. **B223**, 422 (1983).
[4] H. B. Li, J. Phys. **G 36**, 085009 (2009).
[5] A. Kupsc, Int. J. Mod. Phys. **E 18**, 1255 (2009).
[6] J. Gasser and H. Leutwyler, Nucl. Phys. **B250**, 465 (1985); H. Neufeld and H. Rupertsberger, Z. Phys. **C 68**, 91 (1995).
[7] R. Jora, Nucl. Phys. Proc. Suppl. 207-208, 224 (2010).
[8] R. Escribano, PoS QNP 2012, 079 (2012).
[9] D. Alde *et al.* (GAMS-2000 Collaboration), Z. Phys. **C 36**, 603 (1987).
[10] M. Ablikim *et al.* (BESIII Collaboration), Chin. Phys. **C 36**, 915 (2012).
[11] M. Ablikim *et al.* [BESIII Collaboration], Chin. Phys. **C 41**, 013001 (2017).
[12] M. Ablikim *et al.* (BES Collaboration), Nucl. Instrum. Methods Phys. Res., Sect. **A 614**, 345 (2010).
[13] S. Agostinelli *et al.* (GEANT4 Collaboration), Nucl. Instrum. Methods Phys. Res., Sect. **A 506**, 250 (2003).
[14] D. J. Lange, Nucl. Instrum. Meth. **A 462**, 1 (2001); R. G. Ping, Chin. Phys. **C 32**, 599 (2008).
[15] S. Jadach, B. F. L. Ward and Z. Was, Comput. Phys. Commun. **130**, 260 (2000); Phys. Rev. **D 63**, 113009 (2001).
[16] C. Patrignani *et al.* (Particle Data Group), Chin. Phys. **C 40**, 100001 (2016).

[17] J. C. Chen, G. S. Huang, X. R. Qi, D. H. Zhang, and Y. S. Zhu, Phys. Rev. **D 62**, 034003 (2000).

[18] J. P. Lees *et al.* (BaBar Collaboration), Phys. Rev. **D 88**, 032013 (2013).

[19] S. U. Chung, Phys. Rev. **D 48**, 1225 (1993).

[20] F. Hippel, C. Quigg, Phys. Rev. **D 5**, 624 (1972).

[21] M. Ablikim *et al.* (BESIII Collaboration), Phys. Rev. **D 83**, 012003 (2011).